Modelling Simul. Mater. Sci. Eng. **15** (2007) S361–S375 doi:10.1088/0965-0393/15/4/S04

Computational issues in the simulation of two-dimensional discrete dislocation mechanics

J Segurado[1], J LLorca[1,3] and I Romero[2]

[1] Department of Materials Science, Polytechnic University of Madrid, E T S de Ingenieros de Caminos, 28040 Madrid, Spain
[2] Department of Structural Mechanics, Polytechnic University of Madrid, E T S de Ingenieros Industriales, 28006 Madrid, Spain

E-mail: jllorca@mater.upm.es

Received 3 October 2006, in final form 25 January 2007
Published 1 May 2007
Online at stacks.iop.org/MSMSE/15/S361

Abstract

The effect of the integration time step and the introduction of a cut-off velocity for the dislocation motion was analysed in discrete dislocation dynamics (DD) simulations of a single crystal microbeam. Two loading modes, bending and uniaxial tension, were examined. It was found that a longer integration time step led to a progressive increment of the oscillations in the numerical solution, which would eventually diverge. This problem could be corrected in the simulations carried out in bending by introducing a cut-off velocity for the dislocation motion. This strategy (long integration times and a cut-off velocity for the dislocation motion) did not recover, however, the solution computed with very short time steps in uniaxial tension: the dislocation density was overestimated and the dislocation patterns modified. The different response to the same numerical algorithm was explained in terms of the nature of the dislocations generated in each case: geometrically necessary in bending and statistically stored in tension. The evolution of the dislocation density in the former was controlled by the plastic curvature of the beam and was independent of the details of the simulations. On the contrary, the steady-state dislocation density in tension was determined by the balance between nucleation of dislocations and those which are annihilated or which exit the beam. Changes in the DD imposed by the cut-off velocity altered this equilibrium and the solution. These results point to the need for detailed analyses of the accuracy and stability of the dislocation dynamic simulations to ensure that the results obtained are not fundamentally affected by the numerical strategies used to solve this complex problem.

(Some figures in this article are in colour only in the electronic version)

[3] Author to whom any correspondence should be addressed.

1. Introduction

There is compelling experimental evidence of a size effect on the resistance to plastic flow in metals when the dimensions of the specimen or of the zone subjected to plastic deformation are in the range of a few μm [1–4]. The analysis of this phenomenon is important from the fundamental viewpoint, as the critical deformation and fracture processes in metals take place at this length scale, and because of its implications on the development of micro-electro-mechanical systems and in the micro-electronics industry [5]. The size effects in plasticity were initially observed in conditions of constrained plastic flow (thin films, nanoindentation, torsion, etc) in which strain gradients dominate the response and lead to the presence of geometrically necessary dislocations [1–3]. More recent studies have reported, however, marked size effects in the flow stress unconstrained compression of single crystals [4, 5], which were attributed to a mechanism of dislocation starvation.

The origin of the size effect was traced in both the cases to the inhomogeneous nucleation of individual dislocations upon loading and to the interaction of the dislocation structures with the specimen and/or plastic zone boundaries. Discrete dislocation dynamics (DD), in which the long range elastic interactions between individual dislocations and the influence of the boundary conditions are taken into account within a continuum framework, emerges as the ideal strategy to analyse this phenomenon. An important tool in studies of this kind is the 2D computational model developed by Needleman and Van der Giessen [6], which has been applied to a number of problems including bending of small beams [7], nanoindentation [8], uniaxial deformation of single crystals and polycrystals [9, 10], fracture of confined thin films [11], etc.

Dislocations are 3D entities and it has been argued that 2D models cannot capture many of the complex mechanisms of interaction between dislocations, and that the actual dislocation structures which appear in 3D are different from those found in 2D simulations. Although 3D dislocation dynamic simulations taking into account the boundary conditions have been carried out [12, 13], the computational power required restricts the scope of these simulations to very low strains in configurations which contain a limited number of dislocations. On the contrary, 2D simulations easily treat problems including thousands of dislocations up to strains of 10% and have provided realistic values for the size effect on the plastic flow of single crystals in compression, once the physics of 3D short-range interactions between dislocations are included in the 2D simulations through a set of constitutive rules [14].

More often than not, the limiting factor in the computation of dislocation dynamics in two dimensions is the time step rather than spatial resolution. The original 2D DD framework [6] used an adaptative time-stepping algorithm so that the flight distance of any dislocation during a time step remained within a user-defined maximum distance, which ensured that individual events of dislocation nucleation, dipole annihilation and dislocation pinning by obstacles were taken into account. This strategy led to an average time step below 0.01 ns, which restricted the maximum achievable strain in the simulations to 1% even at very high strain rates ($\approx 10^3\ \mathrm{s}^{-1}$). This limitation was overcome afterwards by using a fixed time step of 0.5 ns and by introducing a cut-off velocity of $20\ \mathrm{m\,s}^{-1}$ for the dislocation speed to reduce the computational burden of following the high velocity oscillatory motions within dislocation pile-ups [7]. As a result, the number of time steps required to reach a given strain was reduced by two orders of magnitude while the overall results were not influenced by these changes in a beam subjected to bending. Since then, simulations based on this model have been carried out following this strategy [8–10, 14], but the validity of these assumptions has not been published in detail and this is the main aim of this investigation.

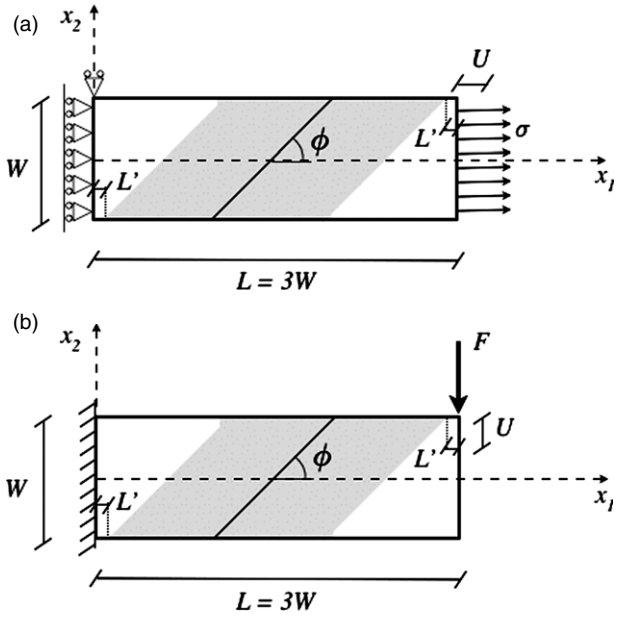

Figure 1. (*a*) Single crystal beam subjected to uniaxial tension. (*b*) Single crystal cantilever subjected to bending. Slip planes oriented at an angle $\phi = 45^\circ$ with the axis x_1 are homogeneously distributed in the shaded areas. The dimensions of the beam in the simulations presented in this paper were characterized by $L = 12\,\mu$m and $L' = L/40$.

2. Discrete dislocation dynamics model

The 2D DD simulations follow the model presented in [6–10] and only the most relevant aspects will be recalled here. Basically, the crystals are taken as isotropic and elastic solids characterized by the elastic modulus E and the Poisson's ratio ν. Plane strain conditions are assumed in the x_1–x_2 plane (figure 1). The crystals have one slip system oriented at $\phi = 45^\circ$ with the positive x_1 axis and are initially free of dislocations. Dislocations are represented by linear singularities perpendicular to the crystal plane with Burgers vector $\boldsymbol{b}$. Dislocation dipoles can be nucleated at discrete points randomly distributed on the slip planes, which mimic the behaviour of Frank–Read sources in 2D, the Burgers vectors $\pm\boldsymbol{b}$ being parallel to the slip plane direction. Nucleation occurs when the magnitude of the resolved shear stress at the source τ exceeds a critical value $\tau_{\rm nuc}$ during a period of time $t_{\rm nuc}$. The distance between the two new dislocations, $L_{\rm nuc}$, is given by

$$L_{\rm nuc} = \frac{E}{4\pi(1-\nu)(1+\nu)}\frac{b}{\tau_{\rm nuc}} \tag{1}$$

so that the resolved shear stress balances the attractive forces between them.

Once generated, dislocations slip in their respective glide planes and the speed V_i of dislocation i is given by

$$V_i = \frac{\tau_i b}{B}, \tag{2}$$

where τ_i stands for the resolved shear stress on the glide plane and B is the drag coefficient. Obstacles to dislocation motion are modelled as a random distribution of points in the glide planes. Dislocations are pinned at these obstacles until the resolved shear stress exceeds

(in absolute value) the obstacle's strength τ_{obs}. Moreover, two dislocations of different signs gliding on the same slip plane are annihilated when they cross each other or if they are within a distance $L_{\text{anh}} = 6b$. Finally, if a dislocation exits the crystal, the dislocation is deleted from the simulation and a displacement jump of $b/2$ is introduced along the slip plane.

The resolved shear stress on the glide plane at the line of dislocation i is computed as

$$\tau_i = \boldsymbol{n}_i \cdot \left[\hat{\boldsymbol{\sigma}} + \sum_{j \neq i} \boldsymbol{\sigma}_j \right] \cdot \boldsymbol{m}_i, \tag{3}$$

with $\boldsymbol{n_i}$ the slip plane normal and $\boldsymbol{m_i}$ the unit vector along the slip plane of dislocation i. $\boldsymbol{\sigma_j}$ stands for the stress induced at the dislocation line for the dislocation j and it is computed analytically from the expressions for the stress field induced by an edge dislocation on an infinite, elastic and isotropic continuum. To this contribution it is necessary to add the field $\hat{\boldsymbol{\sigma}}$ which includes the effect of the image forces induced by the crystal boundaries on the dislocations. At a given stage of loading, the stress-rate and strain-rate fields in the crystal are obtained by the superposition of the two fields, the first one given by the sum of those induced by the individual dislocations in the current configuration and the second one that corrects for the actual boundary conditions. This term is computed by solving a linear elastic boundary value problem using the finite element method with the appropriate boundary conditions, as detailed in [6–10].

The deformation process of the crystal is solved in an explicit incremental manner, using an Euler forward time-integration algorithm for the equations of motion. Once the new positions of all dislocations at time t have been computed, new dislocations are generated at the sources according to (1) and dislocation pairs of opposite sign in the same slip plane are annihilated when they are within L_{anh}. The boundary conditions for the linear elastic boundary value problem are computed from the new dislocation structure and the applied displacements for time $t + \Delta t$. The resolved shear stresses on the dislocations are computed according to (3) from the fields induced by the dislocations and the solution of the boundary value problem. Then, the velocities of the dislocations are obtained from the corresponding resolved shear stress, as given by (2). The new positions are computed from these velocities and the dislocations that meet an obstacle are pinned if the resolved shear stress is below τ_{obs}.

It is important to note that the code is prepared to handle spurious numerical artefacts which appear as a result of the explicit integration scheme. For instance, every time that a dislocation implies that the dislocation has jumped over an obstacle, it is checked if the resolved shear stress is higher than the obstacle strength to avoid dislocations bypassing obstacles. In addition, there is a matrix which keeps track of the relative position of all dislocations gliding in each slip plane. If there is a change in this position during any time step, this means that dislocations of different sign have crossed each other and they are deleted.

2.1. Boundary conditions

Simulations were carried out on beams of length to depth ratio $L/W = 3$ subjected to two different loading conditions: uniaxial tension and bending of a cantilever (figure 1). The boundary conditions for the former are expressed as

$$\begin{aligned} &u_1 = 0, T_2 = 0 \text{ on } x_1 = 0, \\ &u_1 = U, T_2 = 0 \text{ on } x_1 = L, \\ &T_1 = T_2 = 0 \text{ on } x_2 = \pm W/2, \end{aligned} \tag{4}$$

where $T_i = \sigma_{ij} n_j$ is the traction on the boundary with normal n_j. The applied stress σ is computed as

$$\sigma = \frac{1}{W} \int_{-W/2}^{W/2} T_1(L, x_2) \mathrm{d}x_2 \tag{5}$$

to obtain the uniaxial stress–strain curve $(\sigma, U/3W)$. Loading was imposed by applying a constant strain rate of $\dot{\varepsilon} = U/L = 2000\,\mathrm{s}^{-1}$.

The corresponding boundary conditions for the cantilever beam subjected to bending are given by

$$\begin{aligned} &u_1 = u_2 = 0 \text{ on } x_1 = 0, \\ &u_2 = U \text{ on } x_1 = L \text{ and } x_2 = W/2, \\ &T_1 = T_2 = 0 \text{ on } x_2 = \pm W/2 \text{ and } x_1 = L \ (x_2 \neq W/2). \end{aligned} \tag{6}$$

The applied force on the beam end was computed from the shear stresses acting along the beam depth as

$$F = \int_{-W/2}^{W/2} \tau_{12}(0, x_2) \mathrm{d}x_2. \tag{7}$$

Loading was imposed by applying a constant displacement rate $\dot{U}$ of $0.024\,\mathrm{m\,s}^{-1}$ at the cantilever end.

2.2. Material properties

The properties of the material in the simulations were $E = 70\,\mathrm{GPa}$, $\nu = 0.33$ and $b = 0.25\,\mathrm{nm}$. Only one family of slip planes (oriented at an angle of 45° with the positive x_1 axis) was considered, which is shown in the shaded region of figure 1. The distance between consecutive slip planes in this region was 25 nm. The drag coefficient for dislocation glide, $B = 10^{-4}\,\mathrm{Pa\,s}$, was representative of Al [15]. Dislocation sources and obstacles were randomly distributed along the slip planes, the density of both being equal to $56\,\mu\mathrm{m}^{-2}$. The critical resolved shear stress for dislocation nucleation was assigned randomly to the sources following a Gaussian distribution with an average value of $\bar{\tau}_{\mathrm{nuc}} = 50\,\mathrm{MPa}$ and a standard deviation of 1 MPa. The nucleation time for all the sources was $0.01\,\mu\mathrm{s}$. The strength of the obstacles was 150 MPa. These magnitudes are equal to those used in previous simulations [9, 10].

2.3. Finite element analyses

The image stress ($\hat{\boldsymbol{\sigma}}$) and displacement ($\hat{\boldsymbol{u}}$) fields, which account for the effect of the boundary conditions, were computed by the finite element method. These simulations were performed using FEAP [16] with a rectangular grid of 50 by 50 bilinear quadrilateral elements for the beam discretization. The image fields are not singular and this mesh was fine enough; this point was demonstrated by simulations with finer and coarser meshes, which provided very close results. The analyses to determine the image fields were linear and the stiffness matrix of the beam was factorized once, at the beginning of the simulation. Computation of the stresses and displacements in each time step only required the back-substitution with the new boundary conditions

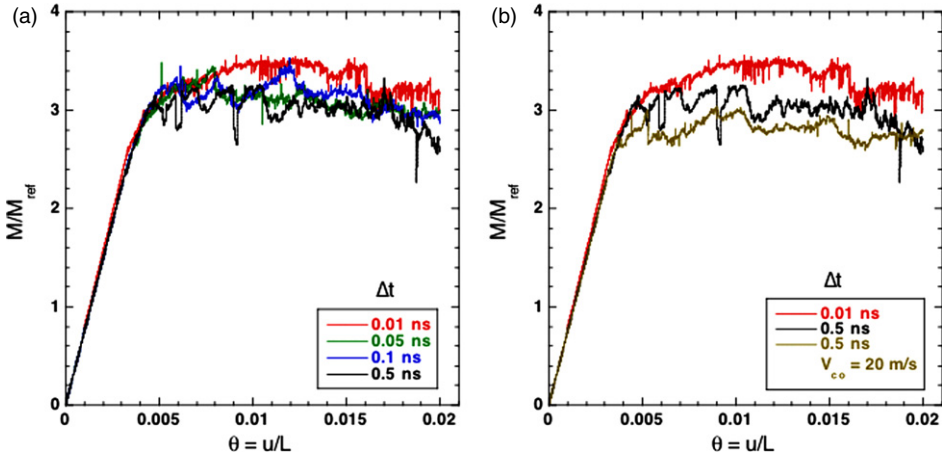

Figure 2. Evolution of the maximum bending moment, M, (normalized by the reference moment M_{ref}) versus maximum rotation angle θ in a microcantilever subjected to bending. (*a*) Influence of the integration time step Δt. (*b*) Influence of the cut-off velocity on dislocation motion.

3. Results and discussion

3.1. Bending

A cantilever beam was chosen to study the behaviour of bending (figure 1(*b*)). Simulations were carried out with time increments in the range 0.01–0.5 ns and the curves of maximum bending moment M versus maximum rotation angle $\theta = U/L$ corresponding to $\Delta t = 0.01$, 0.05, 0.1 and 0.5 ns are plotted in figure 2(*a*). The bending moment was normalized by a reference moment, M_{ref} (as in [7]), which would result from a linear stress distribution of magnitude $\bar{\tau}_{\text{nuc}} x_2/(W/2)$ along the $x_1 = 0$ section of the cantilever. Mathematically

$$M_{\text{ref}} = \frac{2}{W}\int_{-h/2}^{h/2} \bar{\tau}_{\text{nuc}} x_2^2 \, \mathrm{d}x_2 = \frac{1}{6}\bar{\tau}_{\text{nuc}} W^2. \tag{8}$$

The M–θ curves in figure 2(*b*) were practically superposed, and although those computed with longer time increments were rougher, the differences were not significant, in particular if the chaotic nature of dislocation dynamics is taken into account [17]. The dislocation structures at the end of the analysis are plotted in figures 3(*a*) and (*b*) for the simulations carried out with $\Delta t = 0.01$ and 0.5 ns. At first glance, both dislocations' structures show similar features, the dislocations being concentrated in particular planes in which plastic strain was localized, and it should be noted that these results agree qualitatively with the experiments of Motz *et al* [18] on single crystal Cu microbeams manufactured by the focused ion beam technique and tested as cantilevers. Closer analysis of figures 3(*a*) and (*b*) showed some differences in the dislocation structure induced by the differences in the time step. Dislocation nucleation started near the lower axis of the beam and propagated along the slip planes and to the right as the bending moment increased. Simulations carried out with $\Delta t = 0.01$ ns showed the formation of dense dislocation pile-ups which slowed down the propagation of the dislocations along the slip planes towards the upper-right regions of the beam. The dislocation pile-ups in the simulations carried out with $\Delta t = 0.5$ ns were less dense and the dislocations reached the upper-right regions of the beam. These differences were caused by the longer integration time step: the displacement along the slip plane of a dislocation within a pile-up in one time step of 0.5 ns will be 0.1–0.2 μm, assuming that the resolved shear stress acting on a dislocation was

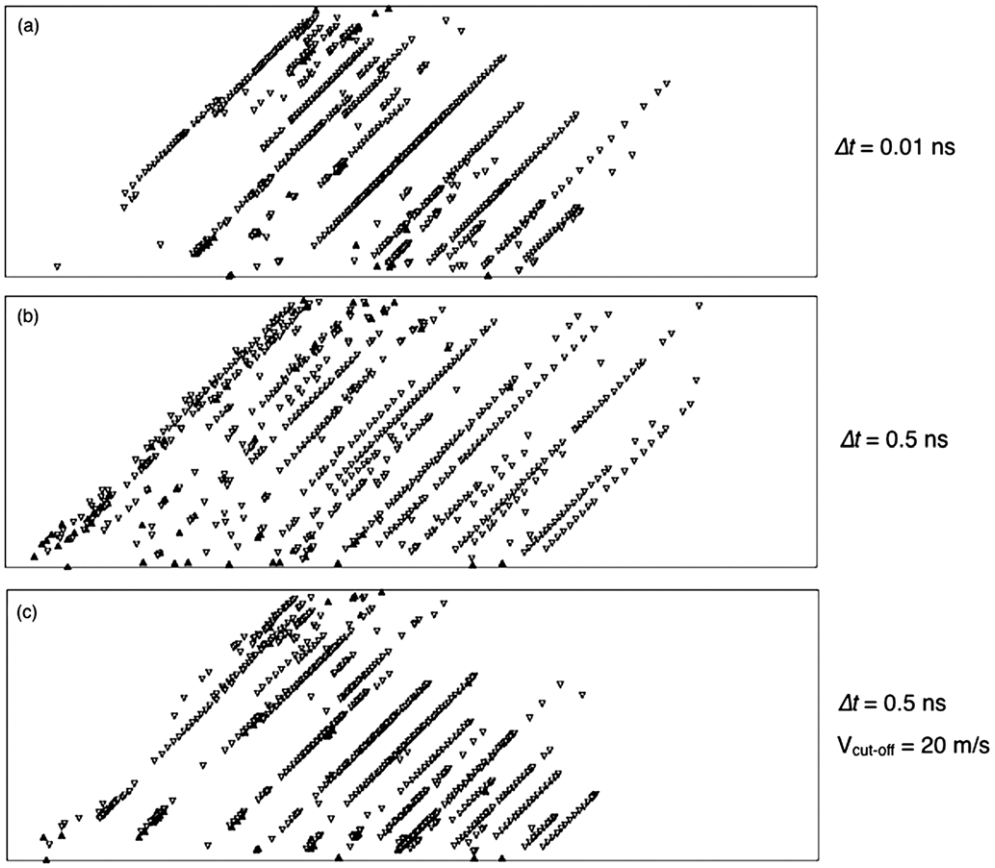

Figure 3. Dislocation structures in a single crystal microcantilever beam subjected to bending at the end of the analysis ($\theta = 5\%$). (*a*) $\Delta t = 0.01$ ns. (*b*) $\Delta t = 0.5$ ns. (*c*) $\Delta t = 0.5$ ns and $V_{\text{cut-off}} = 20\,\text{m}\,\text{s}^{-1}$. Solid and open triangles stand for dislocations of different signs.

in the range $0.5\tau_{\text{obs}}$ to τ_{obs}. As a result, the positions of the dislocations within the pile-ups are very poorly resolved, leading to unrealistic non-equilibrium situations in which the stress acting on the dislocation closer to the obstacle overcame spuriously the obstacle strength and propagated along the slip plane. In addition, dislocations were able to jump over the neutral axis of the beam (in which the applied stresses are low and the driving force for dislocation motion decreased) as a result of the long displacements in each time step, and they reached the upper-right region of the beam. This behaviour was unusual in the simulations carried out at $\Delta t = 0.01$ ns (figure 3(*a*)).

These problems, associated with the long jumps of the dislocations when long integration time steps were used, were cleverly solved by Cleveringa *et al* [7] by introducing a cut-off velocity of $20\,\text{m}\,\text{s}^{-1}$ for the dislocation motion. The results obtained for the bending of the microcantilever in the cases presented in figure 2(*a*) with the minimum (0.01 ns) and maximum (0.5 ns) integration time steps are plotted again in figure 2(*b*) together with those computed with the maximum time step of 0.5 ns and a cut-off velocity of $20\,\text{m}\,\text{s}^{-1}$. These curves show that the cut-off velocity did not modify significantly the M–θ curve, which was very close to the one obtained with $\Delta t = 0.01$ ns and smoother than that computed with $\Delta t = 0.5$ ns without any limit for the dislocation velocity. Moreover, the dislocation structure at the end of the analysis, shown in figure 3(*c*), was very similar to that obtained with $\Delta t = 0.01$ ns.

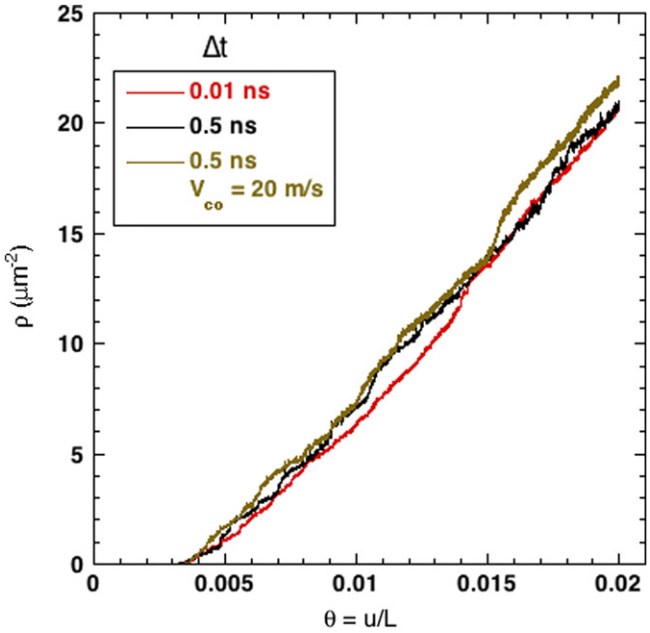

Figure 4. Predictions of the evolution of the dislocation density as a function of the maximum beam rotation θ during bending of a single crystal microcantilever in the simulations in figure 2(*b*).

Obviously, the cut-off velocity reduced the maximum dislocation displacement in each time step by a factor of $\approx$ 20 and the position of the dislocations within the pile-ups were better resolved. The density and the location of the dislocation pile-ups reproduced faithfully the results obtained, at about fifty times the computational cost, with very short integration time steps.

On the basis of these findings, Cleveringa *et al* [7] used longer integration time steps coupled with a cut-off velocity in their dislocation dynamics simulations in bending and further analyses reproduced their strategy in different loading conditions [8–11]. However, it should be noted that bending is a very particular loading mode in which practically all the dislocations are geometrically necessary and thus the dislocation density is controlled by the curvature of the beam. This is shown in figure 4, in which the evolution of the dislocation density with the maximum beam rotation angle is practically superposed in all the simulations plotted in figure 2(*b*). Thus, it seems necessary to explore whether the strategy followed in [7] to increase the integration time step without compromising the outcome of the simulations comes about as an 'intrinsic' behaviour or whether it was conditioned by the deformation mode of the cantilever beam which controlled the total dislocation density.

3.2. Uniaxial tension

The stress–strain curves for the crystals subjected to uniaxial tension up to 5% are plotted in figure 5(*a*) as a function of the time step chosen for the simulations. The overall shape of the curves obtained with Δt in the range 0.01–0.5 ns was very similar: an initial linear elastic region followed by an ideally plastic response. The linear region ended when the first dislocation was nucleated at a far-field applied stress slightly below 100 MPa, which is consistent with the average nucleation strength of 50 MPa taking into account that the Schmidt factor for the

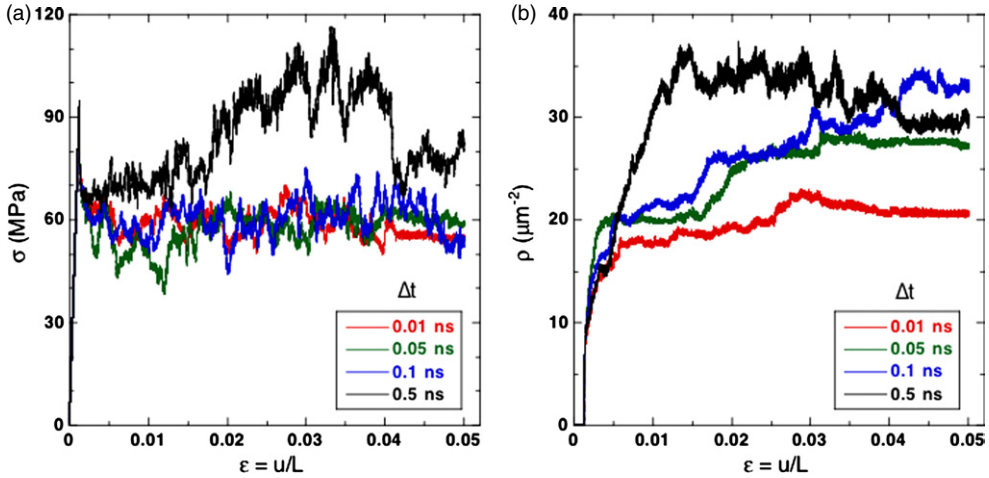

Figure 5. Influence of the integration time step Δt on the simulation of the uniaxial deformation of a single crystal microbeam. (*a*) Stress–strain curve. (*b*) Dislocation density.

slip system is $(\sin 2\phi)/2 = 0.5$. The dislocation density increased sharply after this event (figure 5(*b*)) and reached a steady-state situation, as the number of dislocations nucleated was equivalent to that which exited through the specimen lateral surfaces; the flow stress remained constant under such conditions. The fluctuations in the stress–strain curve increased with the integration time step and were particularly high when $\Delta t = 0.5$ ns, but the overall magnitude of flow stress seemed to converge to the values obtained with shorter time steps at far-field strains of 5%. The evolution of the dislocation density with the applied strain showed similar features (figure 5(*b*)) and more oscillations were found for longer integration time steps. In addition, the dislocation density grew faster and reached higher values at the initial stages of deformation for shorter integration time steps and the steady-state dislocation density at far-field strains of 5% seemed to increase slightly with Δt.

In order to smooth out the mechanical response and maintain long integration times steps, the standard strategy has been to introduce a cut-off velocity in the dislocation motion [8–11]. The results obtained in terms of the stress–strain curve and the evolution of the dislocation density with the applied strain are plotted in figures 6(*a*) and (*b*), respectively. The presence of a cut-off velocity of $20\,\mathrm{m\,s^{-1}}$ for the dislocations reduced dramatically the oscillations in the stress–strain curve and the average value of the flow stress, which was closer to the one computed with the shortest time step of 0.01 ns. However, the simulations with a cut-off velocity of $20\,\mathrm{m\,s^{-1}}$ severely overestimated (by a factor of 3.5 at 5% applied strain) the dislocation density in comparison with the predictions of the models without cut-off velocity.

Thus, introducing a cut-off velocity for the dislocations reduced the oscillations in the stress–strain curve but overestimated the dislocation density. Moreover, the dislocation structures changed with the integration time step and were dramatically altered by the introduction of a cut-off velocity of $20\,\mathrm{m\,s^{-1}}$. This is shown in figure 7 in which the dislocation structures are plotted at $\varepsilon = 5\%$ for the simulations performed with $\Delta t = 0.01$ ns, $\Delta t = 0.5$ ns and $\Delta t = 0.5$ ns and a cut-off velocity of $20\,\mathrm{m\,s^{-1}}$. The simulations carried out with the shortest time increment showed a limited number of active slip planes during the tensile deformation of the single crystal, figure 7(*a*). The plastic deformation was mainly localized in these planes in which dislocation pile-ups developed. The positions of the dislocations within the pile-ups could not be computed accurately in simulations carried out with longer Δt (figure 7(*b*)) and

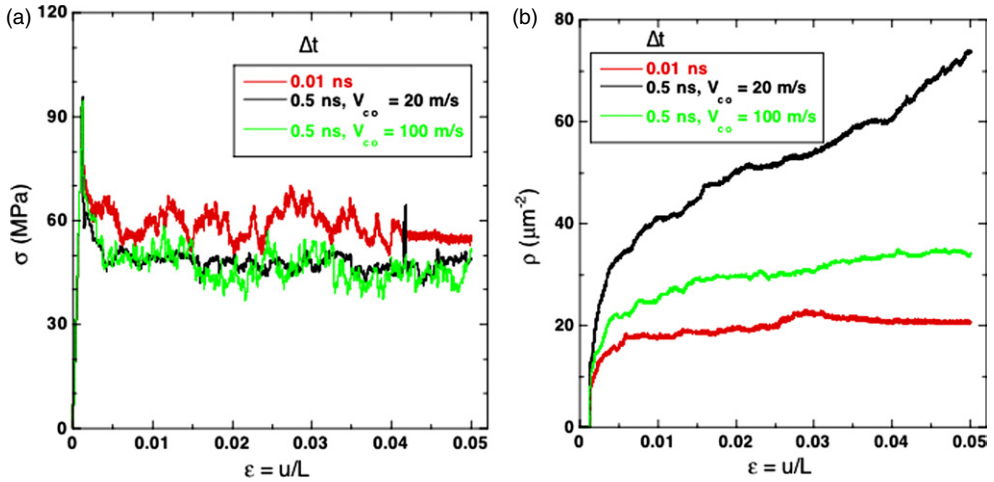

Figure 6. Influence of the dislocation cut-off velocity on the simulation of the uniaxial deformation of a single crystal microbeam. (*a*) Stress–strain curve. (*b*) Dislocation density.

this led to the development of non-equilibrium situations which increased sharply the stresses acting on the dislocation closest to the obstacle. As a result, the dislocation pile-ups were unstable and the dislocations could not be stopped by the obstacles and propagated along the slip planes, generating more dislocations in other planes and increasing the dislocation density.

Imposing a cut-off velocity of $20\,\mathrm{m\,s^{-1}}$ on the simulations carried out with $\Delta t = 0.5$ ns changed completely the dislocation pattern (figure 7(*c*)). Long dislocation pile-ups were formed in several slip planes and this led to noticeable differences in the deformation of the beam between the simulations carried out with the shortest time step of 0.01 ns (figure 8(*a*)) and those performed at the longest time step of 0.50 ns with a cut-off velocity of $20\,\mathrm{m\,s^{-1}}$ for the dislocations (figure 8(*b*)). In the absence of a cut-off velocity, plastic deformation was concentrated in a couple of slip planes in which successive dislocations were nucleated, propagated and left the crystal. The cut-off velocity generated long and dense pile-ups and more dislocations were stored in the crystal. The stress field generated by the pile-ups nucleated dislocations in nearby slip planes and the plastic deformation was spread over a wider region.

It has been shown in previous investigations that dislocation dynamics is chaotic [17] and that the predictions obtained with dislocation dynamics are very sensitive to the details of the simulations, such as the precise location of sources and obstacles, particularly when the behaviour is dominated by statistical stored dislocations. In order to ensure that the results presented in figures 6 and 7 are general, three simulations were carried out with and without a cut-off velocity with different distributions of dislocations and sources. The predictions of the dislocation density as a function of the applied strain are plotted in figure 9, and they show that in all the cases the densities obtained with a cut-off velocity of $20\,\mathrm{m\,s^{-1}}$ were about 3 to 4 times higher.

These differences are obviously a consequence of the cut-off velocity imposed on the dislocations, which alters radically the dislocation dynamics. The effect of this modification can be assessed from the results shown in figure 10(*a*), in which the average dislocation velocity in each time step is plotted as a function of the applied strain in the simulations carried out with $\Delta t = 0.50$ ns. The average speed was computed from all the dislocations in the model, taking into account that the dislocations blocked by an obstacle are assigned null velocity, so that it

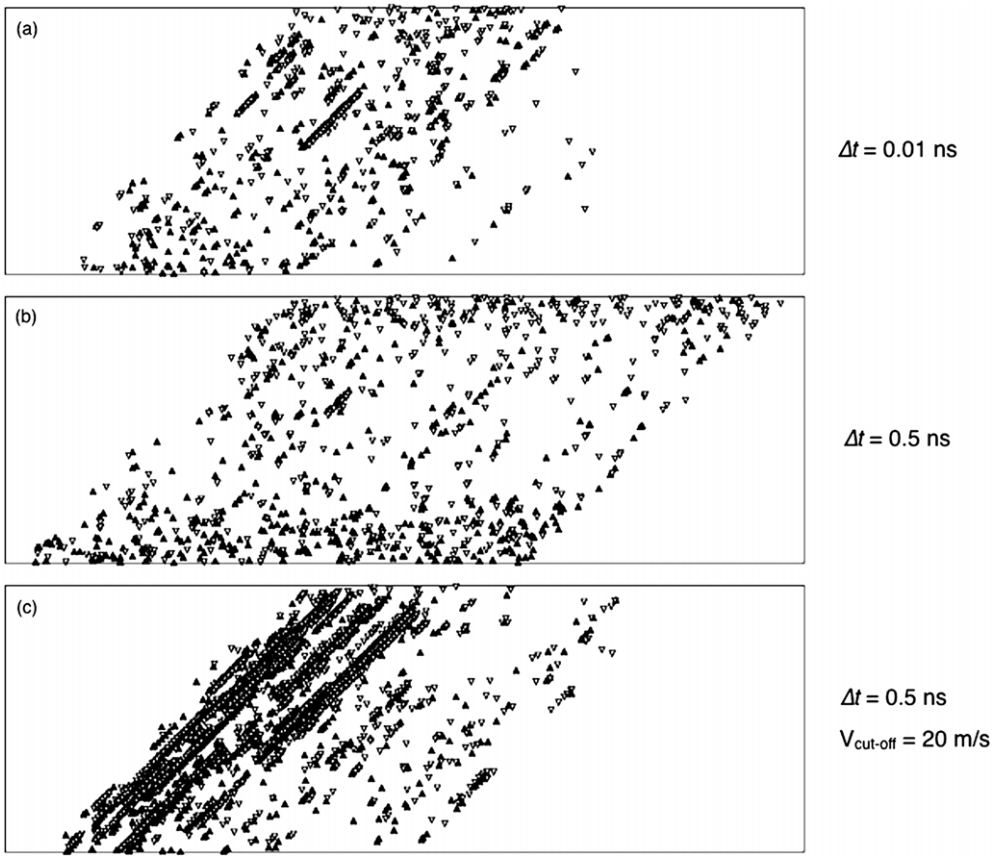

Figure 7. Dislocation structures in a single crystal microbeam subjected to uniaxial tension at the end of the analysis ($\varepsilon = 2\%$). (*a*) $\Delta t = 0.01$ ns. (*b*) $\Delta t = 0.5$ ns. (*c*) $\Delta t = 0.5$ ns and $V_{\mathrm{cut-off}} = 20\,\mathrm{m\,s^{-1}}$. Solid and open triangles stand for dislocations of different signs.

includes the dislocations within pile-ups and those sliding freely along the corresponding slip planes. The spikes with average velocities above $50\,\mathrm{m\,s^{-1}}$ are isolated events corresponding to large instabilities and are not representative of the overall behaviour[4]. Nevertheless, the average dislocation speed is comparable to the cut-off velocity of $20\,\mathrm{m\,s^{-1}}$ most of the time and approximately 50% of the mobile dislocations were slowed down throughout the analysis as a result of this limit to the dislocation speed, figure 10(*b*). A portion of these slowed-down dislocations is within pile-ups and the correction leads to more stable dislocation pile-ups by smoothing out the high-frequency oscillatory motions. However, this correction also affected many dislocations moving freely along slip planes (for instance, after they have broken free from an obstacle), introducing an error in the dislocation dynamics simulations because the forces acting on these dislocation are not used, in fact, to determine the dislocation speed.

Obviously, the higher the cut-off velocity, the lower the number of dislocations slowed down and this should lead to better approximations. Increasing $V_{\mathrm{cut-off}}$ to $100\,\mathrm{m\,s^{-1}}$ led to a stress–strain curve almost superposed on that computed with $V_{\mathrm{cut-off}} = 20\,\mathrm{m\,s^{-1}}$, although with more oscillations (figure 6). The dislocation density was significantly reduced, although

[4] The curve contains 50 000 points and the spikes correspond to a few hundreds of time increments. Its effect is magnified in the plot because of the thickness of the line.

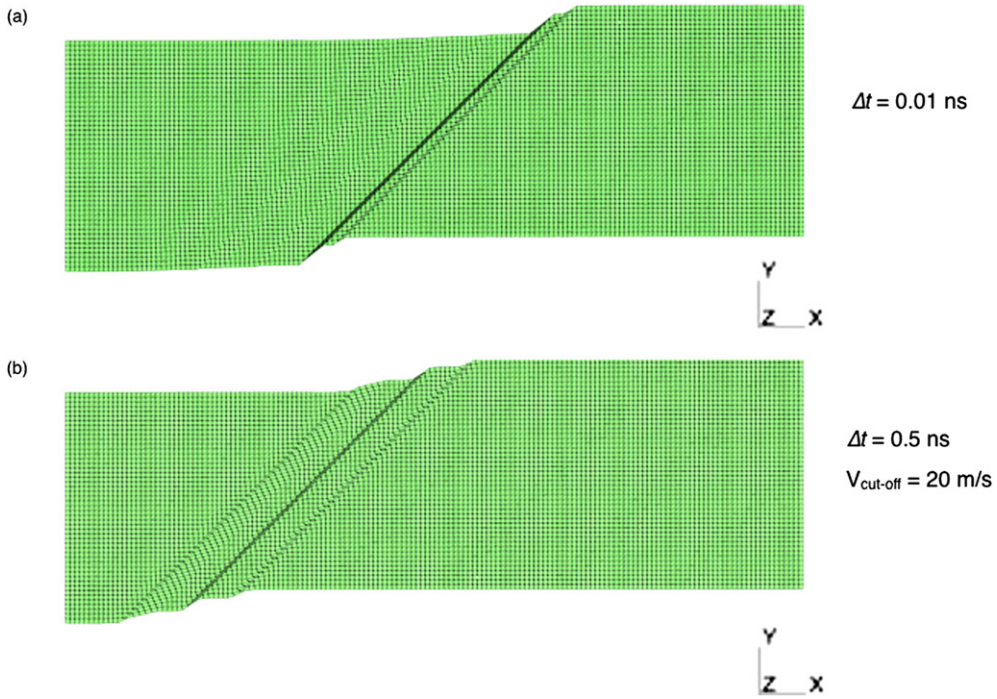

Figure 8. Deformed shape of the single crystal microbeam subjected to uniaxial tension. (*a*) $\Delta t = 0.01$ ns. (*b*) $\Delta t = 0.5$ ns and $V_{\text{cut-off}} = 20\,\text{m}\,\text{s}^{-1}$. The displacement magnification factor was 2.

the steady-state value was almost twice that of obtained in the simulations with $\Delta t = 0.01$ ns. These results are in agreement with the previous discussion and are supported by the changes in the fraction of slowed-down dislocations with the cut-off velocity shown in figure 9(*b*).

In brief, the introduction of the cut-off velocity led to two effects on the dynamics of dislocations. Firstly, the dislocation pile-ups are stabilized by filtering the high-frequency oscillations which led to non-equilibrium situations when long time increments were used. Secondly, it slowed down the overall motion of many dislocations moving freely along the slip planes, and this modified the evolution of the dislocation density with the applied strain. The curves plotted in figure 6(*b*) show that the dislocation density in uniaxial tension grew sharply from the onset of plastic deformation and reached rapidly a steady state due to the balance between the new dislocations generated at the sources and those which were annihilated or exited the crystal through the lateral surfaces. This equilibrium is altered if the velocity of the dislocations moving along the slip planes is reduced and as a result, the dislocation density attained much higher values and—in our simulations—did not reach an equilibrium value. These extra dislocations were accumulated in pile-ups (leading to the localization of deformation in a few slip planes) and their stress fields contributed to the nucleation of more dislocations in nearby slip planes.

The scenario depicted in the previous paragraph was not operative in the beams loaded in bending, because the dislocations were geometrically necessary and the dislocation density was proportional to the plastic curvature of the beam (figure 4). Only the first effect (stabilizing the pile-ups) was operative and the insertion of a cut-off velocity for the dislocation motion was a clever strategy to improve the computational efficiency of the dislocation dynamics

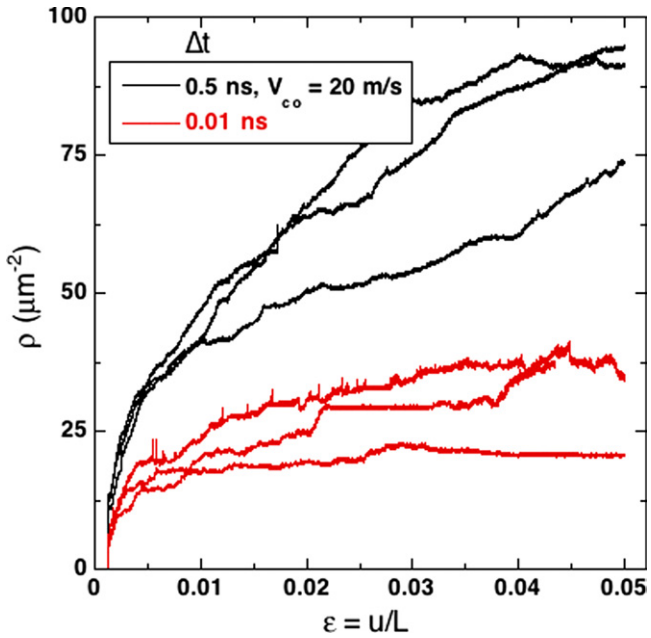

Figure 9. Influence of the initial distribution of sources and obstacles on the dislocation density during uniaxial deformation of a single crystal microbeam. The results are presented for simulations carried out with and without a cut-off velocity of 20 m s^{-1}.

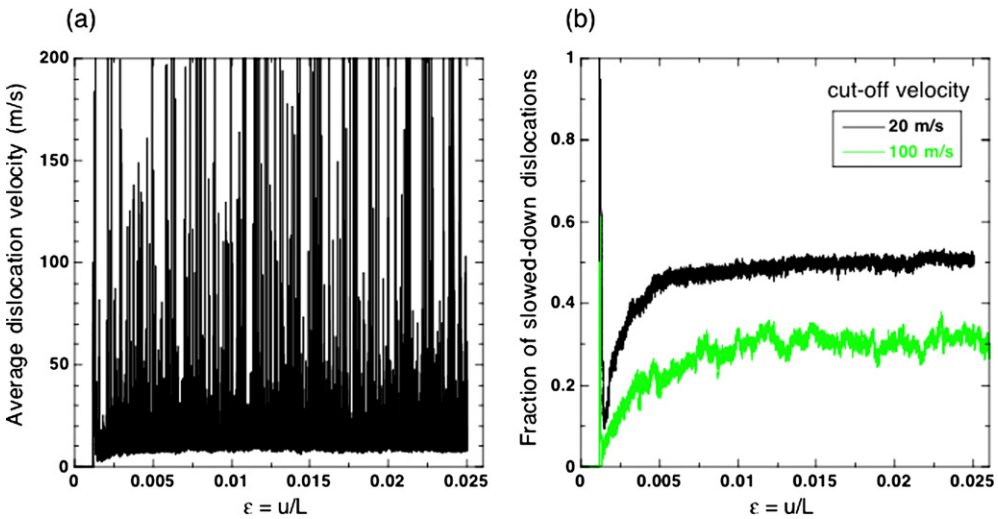

Figure 10. (*a*) Average dislocation velocity in each time increment in the simulations carried out at $\Delta t = 0.5$ ns. (*b*) Fraction of dislocations slowed down in each time step in the simulations carried out at $\Delta t = 0.5$ ns and $V_{\text{cut-off}} = 20$ m s^{-1} or 100 m s^{-1}.

simulations without losing accuracy. In contrast, the dislocation density in uniaxial tension is due to statistically stored dislocations and a reduction of the dislocation speed changes the balance between dislocation nucleation and dislocations exiting the crystal, increasing artificially the dislocation density.

4. Concluding remarks

More often than not, temporal resolution is more critical than spatial resolution to achieve meaningful results (either of fundamental or practical interest) in the numerical modelling of the mechanical behaviour of materials. Two-dimensional discrete dislocation dynamics has emerged in the last decade as an extremely useful tool to analyse size effects in plasticity when the length scales involved are in the range of a few μm. The success of this simulation strategy is partially due to its ability to treat rigorously the effect of complex boundary conditions and to reach large strains (up to 10%) in problems containing hundreds of dislocations. This latter result has benefited from *ad hoc* modifications in the Euler forward time-integration algorithm for the equations of dislocation motion, which allowed longer integration time steps (up to two orders of magnitude) without sacrificing accuracy, by introducing a cut-off velocity for the dislocation motion.

It is well known that explicit time-integration algorithms are not always unconditionally stable and this investigation was aimed at studying the influence of the integration time step size and of the introduction of a cut-off velocity on the numerical results obtained for a beam subjected to bending and uniaxial tension. Increasing the integration time step led in both cases to similar results: a progressive increment of the oscillations in the numerical solution, which would eventually lead to an erroneous solution because the details of the dislocation nucleation and annihilation and of the interactions among dislocations were poorly resolved. These problems were eliminated in the beam subjected to bending by introducing a cut-off velocity for the dislocation speed and the solutions obtained with integration time steps of 50 ns and a cut-off velocity of 20 m s^{-1} were very close to those computed with integration time steps fifty times smaller. However, the same strategy applied to uniaxial tension led to divergent results, particularly in the dislocation density and in the deformation patterns. Basically, the cut-off velocity for the dislocations reduced the rate of dislocations exiting the crystal during deformation and increased by a factor of 3.5 the total number of statistically stored dislocations. These dislocations were arranged in long pile-ups which led to the localization of the plastic deformation in a narrow band of slip planes. This mechanism was not operative, however, in bending because the dislocation density was controlled by the plastic curvature of the beam. These results point out the need of detailed analyses of the accuracy and stability of the dislocation dynamics simulations to ensure that the results obtained are not fundamentally affected by the numerical strategies implemented to solve these complex problems.

Acknowledgments

The financial support from the Comunidad de Madrid through the program ESTRUMAT-CM and the Spanish Ministry of Science and Education through grants DPI2006-14104 and MAT2006-2602 is gratefully acknowledged.

References

[1] Fleck N A, Muller G M, Ashby M F and Hutchinson J W 1994 *Acta Metall. Mater.* **42** 475
[2] Hutchinson J W 2000 *Int. J. Solids Struct.* **37** 225
[3] Uchic M D, Dimiduk D M, Florando J N and Nix W D 2004 *Science* **305** 986
[4] Greer J R, Oliver W C and Nix W D 2005 *Acta Mater.* **53** 1821
[5] Schwarz K W and Chidambarrao D 2005 *Mater. Sci. Eng.* A **400–401** 435
[6] Van der Giessen E and Needleman A 1995 *Modelling Simul. Mater. Sci. Eng.* **3** 689
[7] Cleveringa H H M, Van der Giessen E and Needleman A 1999 *Int. J. Plast.* **15** 837
[8] Widjaja A, Van der Giessen E and Needleman A 2005 *Mater. Sci. Eng.* A **400–401** 456

[9] Deshpande V S, Needleman A and Van der Giessen E 2005 *J. Mech. Phys. Solids* **53** 2661
[10] Balint D S, Deshpande V S, Needleman A and Van der Giessen E 2006 *Modelling Simul. Mater. Sci. Eng.* **14** 409
[11] Chng A C, O'Day M P, Curtin W A, Tay A O A and Lim K M 2006 *Acta Mater.* **54** 1017
[12] Weygand D, Friedman L H, Van der Giessen E and Needleman A 2002 *Modelling Simul. Mater. Sci. Eng.* **10** 437
[13] Groh S, Devincre B, Kubin L P, Roos A, Feyel F and Chaboche J L 2005 *Mater. Sci. Eng.* A **400–401** 279
[14] Benzerga A A and Shaver N F 2006 *Scr. Mater.* **54** 1937
[15] Kubin L P, Canova G, Condat M, Devincre B, Pontikis V and Brechet Y 1992 *Solid State Phenom.* **23–24** 455
[16] Taylor R L 2005 *FEAP, A finite element analysis program, v 7.5*. University of California
[17] Deshpande V S, Needleman A and Van der Giessen E 2001 *Scr. Mater.* **45** 1047
[18] Motz C, Schöberl T and Pippan R 2005 *Acta Mater.* **53** 4269